This article has been accepted for publication in a future issue of this journal, but has not been fully edited. Content may change prior to final publication. Citation information: DOI 10.1109/TAP.2020.3016492, IEEE Transactions on Antennas and Propagation

Frequency Scaling Model for the Prediction of Total Tropospheric Attenuation Time Series at EHF

Lorenzo Luini, *Senior Member*, *IEEE*, Alberto Panzeri, Carlo Riva, *Senior Member*, *IEEE*

***Abstract* — A frequency scaling model aiming to predict total tropospheric attenuation time series at EHF is presented. One version of the model (TAFS) is more accurate but, besides the reference attenuation time series at low frequency, it also requires additional ancillary inputs (e.g. radiometric data and information on the rain drop size distribution); a second version (S-TAFS) is simpler, though at the expenses of a slightly worse performance. Both TAFS and S-TAFS first rely on isolating the attenuation induced by the different atmospheric constituents, each of which is separately up-scaled to the target frequency. The two methods are tested against a full-year of data collected at Ka band and Q band at Politecnico di Milano in the framework of the Alphasat Aldo Paraboni propagation experiment. Results indicate that both methods offer a very good accuracy in scaling the total attenuation from Ka to Q band, both in terms of first-order statistics and of time series. This corroborates the use of TAFS and S-TAFS to predict the total tropospheric attenuation at much higher frequency bands (e.g. the W band), for which no measurements are currently available, starting from the largely available Ka-band measurements.**

***Index Terms* — Tropospheric attenuation, frequency scaling, satellite communications.**

I. Introduction

Several advantages, such as lighter and smaller equipment as well as the availability of a larger bandwidth for more demanding services, induce to deploy communication systems working at higher and higher frequency: indeed, the Q/V band [1], and possibly the W band at a later stage [2], will supplement the use of the Ka band, which is the reference band for modern broadband satellite communication systems. However, in these portions of the spectrum, the impairments caused by the troposphere on radio waves increase rapidly. Thus, it is of paramount importance to use accurate and reliable tools to design systems working at higher frequency bands, such as the W band, for which no measurements are currently available. To this aim, physically-based prediction models need to be privileged, as they are characterized by a better reliability and wider applicability, if compared to empirical methodologies. Furthermore, the optimum prediction method should target separately the attenuation induced by the various tropospheric components (all of which become more and more relevant with the increase in frequency [2]), and it should also allow predicting both first order statistics and time series, the latter being crucial for the design and operation of the necessary fade mitigation techniques when fixed power margins are no longer sufficient to provide the expected system performance [1].

The models available in the literature satisfy just some of the requirements mentioned above, but not all. For example, the total attenuation prediction model adopted by the International Telecommunication Union – Radiocommunication Sector (ITU-R) in Recommendation P.618-13 [3], regarded as one of the most accurate statistical models, actually addresses the attenuation due to rain, clouds and gases, but, on the other hand, its applicability is limited to 55 GHz and it does not allow predicting time series. The latter are generated by time series synthesizers, which, however, are typically of stochastic nature, i.e. are meant to produce realistic time series but not to reproduce real events (see for example the model proposed in [4]). Finally, very high prediction accuracy can be achieved by frequency scaling techniques, which aim at estimating the attenuation at a higher frequency from the attenuation measured at a lower frequency; both accurate statistical and physically-based approaches exist [5]-[11], but they all address only rain attenuation.

This work presents the development of a total tropospheric attenuation prediction model, which is tested against the propagation data collected by the NASA beacon receivers installed at Politecnico di Milano in the framework of the Alphasat Aldo Paraboni propagation experiment [12]. The model relies on the instantaneous frequency scaling of the single components of the tropospheric attenuation, thus filling the current modelling gap in the literature. The first optimal methodology derived from the model, referred to as Total Attenuation Frequency Scaling (TAFS) requires more detailed inputs such as radiometric data and information on the drop dimension, which are used to better isolate the single contributions to the total tropospheric attenuation at lower frequency; the second simplified methodology (referred to as Simplified Total Attenuation Frequency Scaling − S-TAFS)

Manuscript received XXXX.

Lorenzo Luini and Carlo Riva are with the Dipartimento di Elettronica, Informazione e Bioingegneria, Politecnico di Milano, Piazza Leonardo da Vinci, 32, 20133, Milano, Italy, and with the Istituto di Elettronica e di Ingegneria dell'Informazione e delle Telecomunicazioni (IEIIT), Consiglio Nazionale delle Ricerche, Via Ponzio 34/5, Milano 20133, Italy (e-mail: lorenzo.luini@polimi.it).

Alberto Panzeri is with the Dipartimento di Elettronica, Informazione e Bioingegneria, Politecnico di Milano, Piazza Leonardo da Vinci, 32, 20133, Milano, Italy.

This article has been accepted for publication in a future issue of this journal, but has not been fully edited. Content may change prior to final publication. Citation information: DOI 10.1109/TAP.2020.3016492, IEEE Transactions on Antennas and Propagation

provides slightly less accurate results, but it requires simpler input data that are more readily available on a Global basis.

Following this introduction, Section II describes the experimental setup and how the measured data are pre-processed to be used with TAFS and S-TAFS; Section III and Section IV present in detail the development and the main features of TAFS and S-TAFS, respectively. The accuracy of both methods is evaluated in Section V using measurements at Q band, while Section VI draws some conclusions.

II. Experimental Setup and Data Processing

Fig. 1 gives an overview of all the experimental instruments deployed on the rooftop of Building 20 of Politecnico di Milano. More details on such equipment are given in the following subsections.

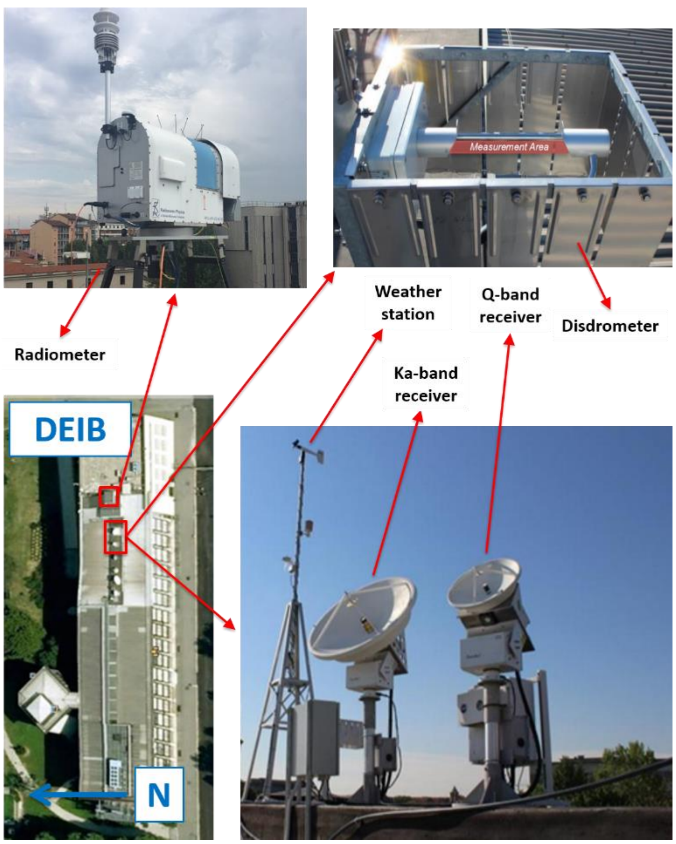

Fig. 1. Experimental instruments installed on the rooftop of the Dipartimento di Elettronica, Informazione e Bioingegneria (DEIB) of Politecnico di Milano.

A. Alphasat Ka/Q-Band Beacon Receivers

The frequency scaling methods presented in this work are tested against the measurements collected in the framework of the Alphasat Aldo Paraboni propagation experiment, a joint collaboration between the Italian Space Agency (ASI) and the European Space Agency (ESA). The experimental campaign aims at investigating the Ka, Q and V bands along Earth-space links. The Alphasat satellite, launched on July 25th, 2013 and positioned on a geosynchronous orbit (25° E longitude), carries the Aldo Paraboni payload, which includes two coherent continuous-wave beacons operating at 19.701 GHz (Ka band) and 39.402 GHz (Q band).

The Ka band signal has linear vertical polarization, while the Q band one is also linearly polarized, but with a 45° tilt angle. The received beacon power is collected at 8 samples/second by two receivers installed on the rooftop of Building 20 in the main campus of Politecnico di Milano, Italy (latitude 45.48° N, longitude 9.23° E, altitude 137 m a.m.s.l.), as shown in Fig. 1. The antennas have a diameter of 1.2 m (Ka band) and 0.6 m (Q band), and the Alphasat satellite is tracked based on the satellite ephemeris provided by Inmarsat on a weekly basis. Both receivers have a dynamic range of approximately 35 dB. Finally, the average elevation angle of the link is 35.6°.

B. Disdrometer

The Thies Clima disdrometer observes hydrometeors to classify them in terms of their dimension, falling speed and type (e.g. rain, snow, hail, …) using a 785-nm laser beam. The disdrometer divides hydrometeors in 22 diameter classes (0.125 mm-8 mm) and 20 velocity classes (0 m/s-10 m/s). The Drop Size Distribution (DSD), $N(D)$ (mm^{-1} m^{-3}), i.e. the number of particles with given diameter D per m^3 [13], is calculated as follows:

$$N(D_i) = \frac{10^6\, n_i}{S\ v(D_i)\, T\, \Delta D_i} \quad (1)$$

where n_i is the number of raindrops with diameter falling in the i-th bin (with average diameter D_i), ΔD_i (mm) is the dimension of each size bin, S (mm^2) denotes the disdrometer sampling area, $v(D_i)$ (m/s) is the terminal particle speed, T(s) is the instrument integration time.

The precipitation intensity R (mm/h) is obtained from the DSD as:

$$R = 600 \cdot 10^{-6} \pi \sum_{i=1}^{N} N(D_i) D_i^3 v(D_i) \Delta D_i \quad (2)$$

The disdrometer outputs are provided in 1-minute intervals.

C. Radiometer

A multi-channel microwave radiometer (MWR), pointing to the Alphasat satellite, supports the propagation experiment in Milan. Specifically, the instrument, manufactured by Radiometer Physics GmbH, measures the sky noise (also commonly referred to as the brightness temperature) at two channels in the Ka band (23.84 and 31.4 GHz) and two channels in the W band (72.5 and 82.5 GHz), which, in turn, is used to estimate the tropospheric attenuation in rain-free conditions using simple well-established algorithms [14].

D. Weather Station

The meteorological sensors, also property of NASA, collect data on the surface values of pressure, temperature and relative humidity with sampling time of 1 minute. As a backup for the meteorological measurements, a second weather station is installed on the radiometer.

E. Radiosonde Observations

The experimental dataset is completed by 20 years of vertical profiles of the atmosphere, namely pressure P, relative humidity RH and temperature T, obtained from the radiosonde observations (RAOBS) carried out twice a day at Milano Linate Airport (5 km from the experimental site).

This article has been accepted for publication in a future issue of this journal, but has not been fully edited. Content may change prior to final publication. Citation information: DOI 10.1109/TAP.2020.3016492, IEEE Transactions on Antennas and Propagation

III. The Total Attenuation Frequency Scaling (TAFS) Method

The Total Attenuation Frequency Scaling (TAFS) method, presented in detail in this Section, consists in two consecutive steps: first, the separation of the tropospheric attenuation at frequency f_D into its various components due to the different atmospheric constituents (i.e. attenuation due to rain, clouds and gases); second, the attenuation up-scaling from f_D to f_U, performed separately for each component.

A. Separation of the Tropospheric Attenuation Components Using TAFS

Gases, clouds and hydrometeors are the tropospheric constituents interacting with electromagnetic waves in the 1-1000 GHz frequency range. The first goal of TAFS is to obtain from the total tropospheric attenuation A the contributions due to oxygen (A_{OX}), water vapor (A_V), cloud (A_C), and rain (A_R). The total tropospheric attenuation $A(f_D)$ is derived from the 19.701 GHz beacon received power, P_B, by taking advantage of the collocated MWR, which allows estimating, with very high accuracy, the tropospheric attenuation in non-rainy conditions A^{MWR}, starting from brightness temperature T_B measured in (at least) two channels. Details on the method to derive A from P_B, already applied in many experimental campaigns (e.g. [15]), are fully given in [14].

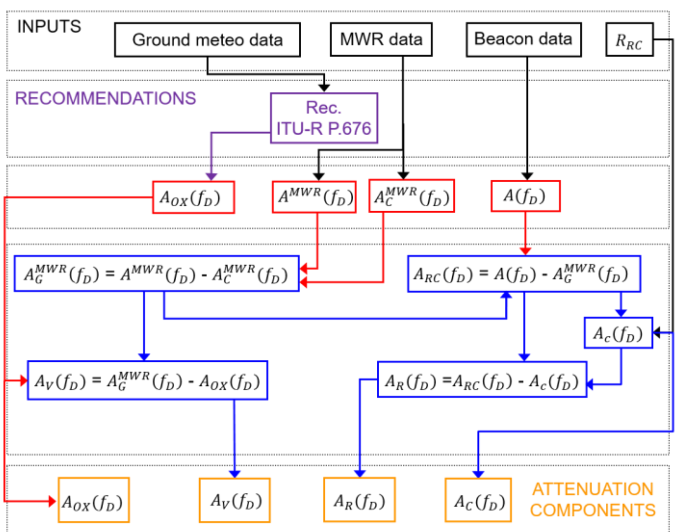

Fig. 2. First part of TAFS: derivation of the attenuation due to oxygen, water vapor, cloud and rain from the time series of $A(f_D)$.

The process to separate A into its contributions, summarized in Fig. 2 and briefly recalled hereinafter, was conceived in [16], to which the reader is addressed for further details.

To derive the attenuation due to the different tropospheric constituents, first, scintillations are removed from the total attenuation by low-pass filtering A using the customary cut-off frequency of 0.03 Hz. Afterwards, the gaseous (i.e. oxygen and water vapor) attenuation A_G^{MWR} is isolated by subtracting the cloud attenuation A_C^{MWR} from the MWR-derived total tropospheric attenuation A^{MWR}:

$$A_G^{MWR} = A^{MWR} - A_C^{MWR} = A^{MWR} - a_L L \tag{3}$$

As is clear from (3), A_C^{MWR} is calculated by multiplying the liquid water mass absorption coefficient $a_L(f)$ and the liquid water content integrated along the path L; derived from [17], a_L(19.701 GHz) is 0.391 dB/mm, while L comes again from inverting brightness temperature data using the well-established methodology reported in [18]. As the radiometric estimation of L is accurate only in scattering-free conditions [18], the value of A_G^{MWR} is interpolated between the beginning and the end of each rain event. As outlined in [16], the attenuation due to rain plus clouds A_{RC} is obtained as:

$$A_{RC} = A - A_G^{MWR} \tag{4}$$

while the attenuation due to clouds A_C and the one due to rain A_R are calculated as [16]:

$$A_C = \begin{cases} R_{RC}\, A_{RC} & A_{RC} \le A_{RC}^{max} \\ A_C^{max} & A_{RC} > A_{RC}^{max} \end{cases} \tag{5}$$

$$A_R = A_{RC} - A_C \tag{6}$$

where the cloud attenuation ratio R_{RC} is defined as:

$$R_{RC} = a\, exp(-b\, A_{RC}) + (1-a)\, exp(-c\, A_{RC}) \tag{7}$$

Fig. 2 shows the trend of R_{RC} at 19.7 GHz, while Table I lists the coefficients a, b, c, and the values of A_C^{max} and of A_{RC}^{max} in (5), determined in [16], to which the reader is addressed for more details. Here, it is sufficient to recall that the abovementioned coefficients in (5) and (7) were identified by optimizing the agreement between the complementary cumulative distribution function (CCDF) of A_C obtained from (5), using a full year of beacon-derived attenuation data A, and the same CCDF calculated from the RAOBS data mentioned in Section II.E. To this aim, as performed in [18], vertical profiles of *P-RH-T* obtained from RAOBS were used first to derive the liquid water content by means of the TKK cloud detection algorithm [19], and, afterwards, to calculate the cloud attenuation through the Liebe MPM93 mass absorption model [20].

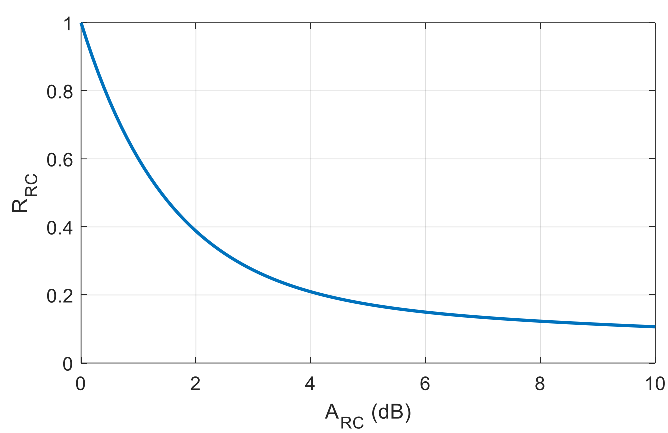

Fig. 3. Trend of R_{RC} as a function of A_{RC} at 19.701 GHz (Ka band).

TABLE I. Coefficients in (7) and Values in (5).

	a	b	c	A_C^{max}	A_{RC}^{max}
19.701 GHz	0.8089	0.6552	0.05958	1.1 dB	11 dB

The attenuation due to oxygen is estimated using the collocated ground meteorological measurements (pressure P and temperature T) as input to the approximate (yet very accurate) prediction model included in Annex 2 of the Recommendation ITU-R P.676-12: this method estimates $A_{OX}(f_D)$ by multiplying the specific attenuation at ground level by the equivalent height, both of which depend on the frequency f, and on the surface values of P and T. As a final step, the attenuation due to water vapor is simply obtained as:

$$A_V(f_D) = A_G^{MWR}(f_D) - A_{OX}(f_D) \quad (8)$$

As an example of the procedure defined in [16] to isolate the different contributions to the total attenuation, Fig. 4 shows the time series of A_G, A_C and A_R for the Ka-band attenuation on the 4th of February, 2017.

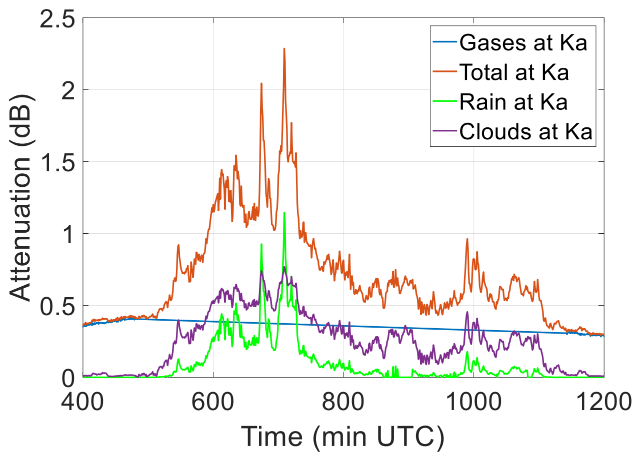

Fig. 4. Separation of the total attenuation (red curve) into its various contributions due to gases (blue curve), clouds (violet curve) and rain (green curve) at 19.701 GHz, using TAFS (4th of February, 2017).

B. Frequency Scaling Using TAFS

In this work, TAFS is applied to scale the Alphasat Ka band attenuation data (f_D = 19.701 GHz) to the Alphasat Q band frequency (f_U = 39.402 GHz), so as to assess the method's accuracy using as reference the Q band data collected in the framework of the same experiment (see Section II.A). More specifically, as summarized in Fig. 5, the application of TAFS consists in scaling separately the time series of $A_C(f_D)$, $A_R(f_D)$, $A_{OX}(f_D)$ and $A_V(f_D)$ using the physically-based approaches explained hereinafter in this Section, which are afterwards summed up to obtain the total attenuation $A(f_D)$.

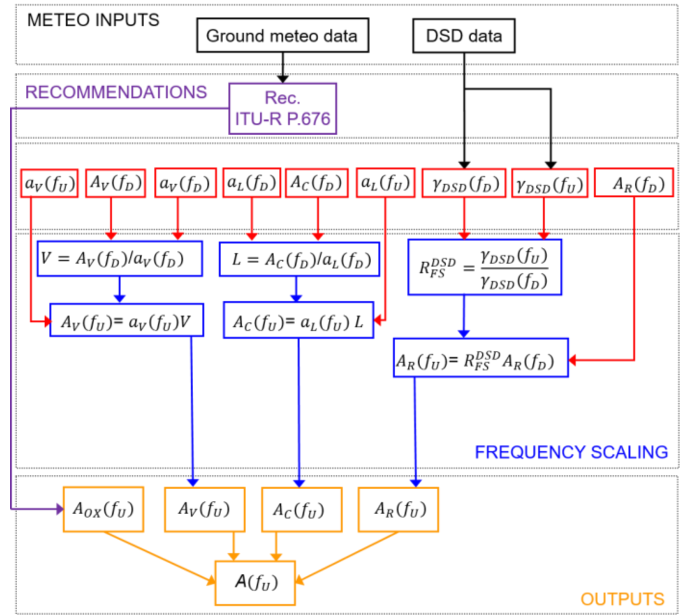

Fig. 5. Second part of TAFS: frequency scaling, from f_D to f_U, of the attenuation due to oxygen, water vapor, cloud and rain.

1) Oxygen Attenuation

Similarly to what is done for $A_{OX}(f_D)$, also $A_{OX}(f_U)$ is estimated using the ground meteorological measurements (P and T) as input to the Recommendation ITU-R P.676-12 [21]. An example of oxygen attenuation time series is shown in Fig. 6, both at 19.701 GHz and 39.402 GHz, for the 4th of February, 2017.

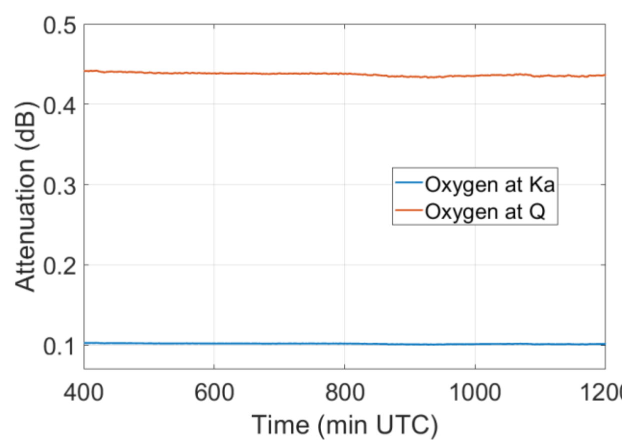

Fig. 6. Scaling the oxygen attenuation from 19.701 GHz (Ka band, blue curve) to 39.402 GHz (Q band, red curve) using TAFS (4th of February, 2017).

2) Water Vapor Attenuation

The attenuation due to water vapor is up-scaled in frequency by taking advantage of the mass absorption coefficient a_V. In fact, the integrated water vapor content along the slant path, V, is derived from the water vapor attenuation $A_V(f_D)$ as follows:

$$V = \frac{A_V(f_D)}{a_V(f_D)} \quad (9)$$

Afterwards, V is multiplied by the water vapor mass absorption coefficient at the high frequency, $a_V(f_U)$ to calculate $A_V(f_U)$:

This article has been accepted for publication in a future issue of this journal, but has not been fully edited. Content may change prior to final publication. Citation information: DOI 10.1109/TAP.2020.3016492, IEEE Transactions on Antennas and Propagation

$$A_V(f_U) = a_V(f_U)\,V \tag{10}$$

The water vapor mass absorption coefficients, which are listed in Table II, are calculated by means of ten years of radiosonde observations (RAOBS) data collected at Milan/Linate airport (45.26° N, 9.17° E, 122 m a.m.s.l., approximately 5 km from the site where the Alphasat beacon receivers are installed), which are used as input to the Liebe MPM93 mass absorption model to calculate the water vapor attenuation [20]. The mass absorption coefficients a_V are derived as the slope of the line fitting the data on the A_V/V plane; the procedure is summarized in Fig. 7. When RAOBS data are not available, a_V can be calculated using the model proposed in [22], which also shows that the variability of the water vapour mass absorption coefficient across different sites is negligible.

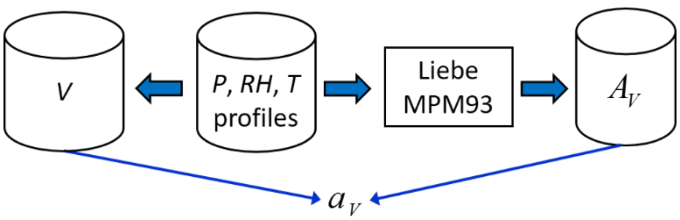

Fig. 7. Procedure to calculate a_V from RAOBS data.

TABLE II. WATER VAPOR MASS ABSORPTION COEFFICIENT VALUES AT DIFFERENT FREQUENCIES.

	Water vapor mass absorption coefficient a_V
19.701 GHz	0.0119 dB/mm
39.402 GHz	0.0105 dB/mm

As an example, Fig. 8 shows the trend of $A_V(f_D)$ and $A_V(f_U)$ for the 4th of February, 2017; as already mentioned, during the rain event, $A_V(f_D)$ is linearly interpolated, and so is also $A_V(f_U)$.

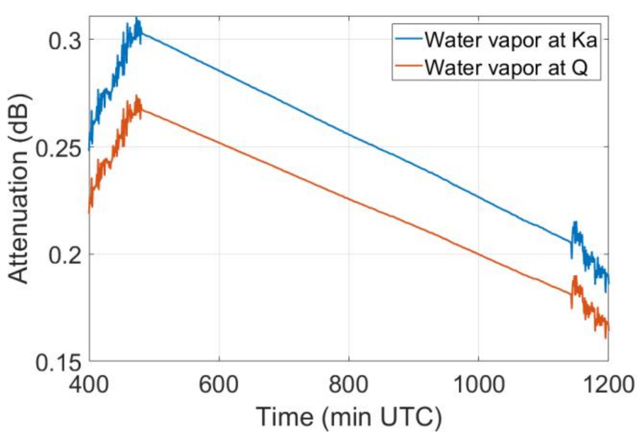

Fig. 8. Scaling the water vapor attenuation from 19.701 GHz (Ka band, blue curve) to 39.402 GHz (Q band, red curve) using TAFS (4th of February, 2017).

3) *Cloud Attenuation*

Similarly to the attenuation due to water vapor, cloud attenuation is linearly related to the integrated liquid water content in clouds L, through the liquid water mass absorption coefficient a_L. Thus, the first step is to derive L along the path as follows:

$$L = \frac{A_C(f_D)}{a_L(f_D)} \tag{11}$$

Afterwards, $A_C(f_U)$ can be easily calculated as

$$A_C(f_U) = a_L(f_U)\,L \tag{12}$$

The calculation of the liquid water mass absorption coefficients is achieved again by exploiting the RAOBS data mentioned in the previous Section, which, as a first step, are provided as input to the TKK model to identify clouds, quantify the liquid water content w, and hence L, by vertical integration [19]. Afterwards, as detailed in Fig. 9, a_L is calculated through the linear regression of the A_C/L scatterplot, where A_C is calculated using the Liebe MPM93 mass absorption model. The values of a_L are listed in Table III. When RAOBS data are not available, a_L can be calculated using the model proposed in [23] (also adopted in recommendation ITU-R recommendation P.840-7 [17]), which also shows that the variability of the liquid water mass absorption coefficient across different sites is negligible.

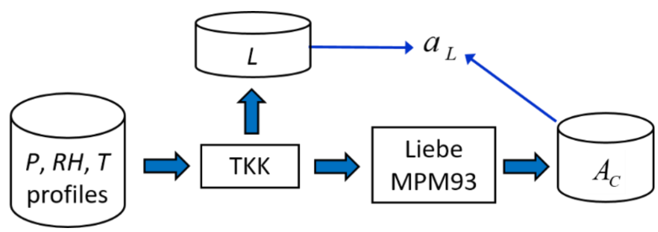

Fig. 9. Procedure to calculate a_L from RAOBS data.

As an example, Fig. 10 shows the trend of $A_C(f_D)$ and $A_C(f_U)$ for the 4th of February, 2017.

TABLE III. LIQUID WATER MASS ABSORPTION COEFFICIENT VALUES AT DIFFERENT FREQUENCIES.

	Liquid water mass absorption coefficient a_L
19.701 GHz	0.391 dB/mm
39.402 GHz	1.338 dB/mm

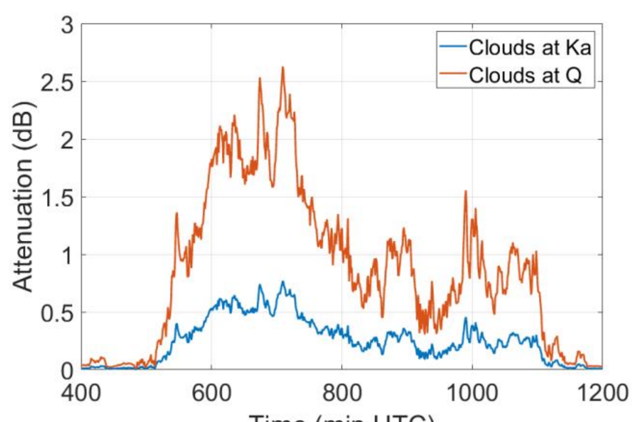

Fig. 10. Scaling the cloud attenuation from 19.701 GHz (Ka band, blue curve) to 39.402 GHz (Q band, red curve) using TAFS (4th of February, 2017).

4) *Rain Attenuation*

Scaling rain attenuation is not a trivial task due to its high variability in space and time; some frequency scaling

This article has been accepted for publication in a future issue of this journal, but has not been fully edited. Content may change prior to final publication. Citation information: DOI 10.1109/TAP.2020.3016492, IEEE Transactions on Antennas and Propagation

approaches for rain attenuation exist in the literature but they are mostly used on a statistical basis. When time series are taken into account, as shown in [16] and [10], the best approach to scale rain attenuation is to rely on the Drop Size Distribution $N(D)$, which is measured, on a 1-minute basis, by the disdrometer collocated with the Alphasat beacon receivers (see Section II.B). In fact, the DSD is tightly linked to the specific attenuation due to rain γ:

$$\gamma(f) = 4.343 \cdot 10^3 \frac{\lambda^2}{\pi} \sum_{i=1}^{N} \mathrm{Re}[S_0(D_i, f)] N(D_i) \Delta D_i \quad (13)$$

In (13) λ is the wavelength, $N = 22$ is the number of diameter classes measured by the disdrometer, and S_0 is the forward scattering coefficient calculated using the T-matrix approach [24] assuming the axial ratio defined by Beard and Chuang in [25]. Based on (13), the frequency scaling ratio is defined as

$$R_{FS} = \frac{\gamma(f_U)}{\gamma(f_D)} \quad (14)$$

and rain attenuation is scaled as

$$A_R(f_U) = R_{FS}\, A_R(f_D) \quad (15)$$

Thanks to (14) and (15), it is therefore possible to take in due account the fast variability of rain attenuation, i.e. the fast temporal evolution of the DSD. As an example, Fig. 11 shows the trend of $A_R(f_D)$ and $A_R(f_U)$ for the 4th of February, 2017.

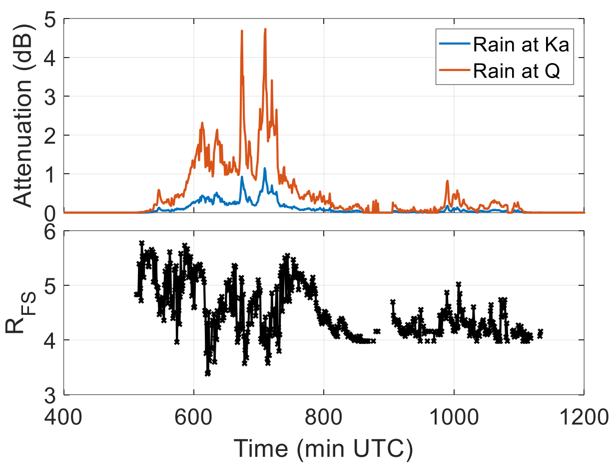

Fig. 11. Top: scaling the rain attenuation from 19.701 GHz (Ka band, blue curve) to 39.402 GHz (Q band, red curve) using TAFS (4th of February, 2017); bottom: corresponding trend of R_{FS}.

5) *Total Attenuation*

As a final step, the time series of total attenuation at frequency f_U is calculated by simply summing the time series of the different attenuation components:

$$A(f_U) = A_{OX}(f_U) + A_V(f_U) + A_C(f_U) + A_R(f_U) \quad (16)$$

As an example, Fig. 12 depicts the trend of the total tropospheric attenuation at frequencies f_D and f_U, along with the single components, for the 4th of February, 2017.

Starting for example from a database of long term total attenuation measurements at lower frequency, the TAFS method is useful to generate, with high accuracy, simulated time series at higher frequencies (and the associated statistics), which can be used to design satellite systems or to simulate fade mitigation techniques.

The accuracy of TAFS in scaling A is presented in Section V, after introducing, in Section IV, a simplified frequency scaling approach (inspired by TAFS), which requires as input data that are more easily retrievable on a Global basis.

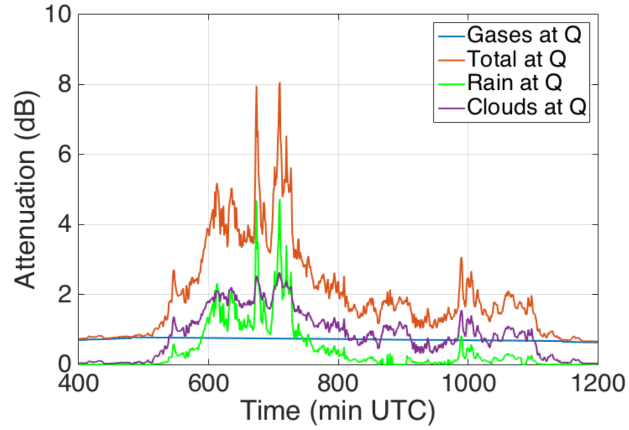

Fig. 12. Gases (blue curve), clouds (violet curve), rain (green curve) and total attenuation (red curve) at 39.402 GHz scaled using TAFS from the corresponding values at 19.701 GHz (4th of February, 2017).

IV. The Simplified Total Attenuation Frequency Scaling (S-TAFS)

As reported in Section V, TAFS offers a very good accuracy in scaling the total tropospheric attenuation but relies on data collected by a radiometer and a disdrometer, whose availability is typically limited to just few sites. This Section introduces a simpler method, Simplified Total Attenuation Frequency Scaling (S-TAFS), which is based on the same principles but is less demanding in terms of inputs, and yet provides a good prediction accuracy.

A. Separation of the Tropospheric Attenuation Components Using S-TAFS

As for TAFS, the key input to S-TAFS are the time series of total tropospheric attenuation at the lower frequency (Ka band), which are low-pass filtered to remove scintillations: in fact, in absence of a collocated radiometer, other methodologies are available to derive the total tropospheric attenuation from beacon data using alternative approaches that rely on simple ancillary data, such as meteorological measurements on the ground, and V values obtained from GNSS receivers and/or NWP products [26].

Given the unavailability of radiometric data, the time series of the attenuation due to oxygen and water vapor are estimated by using directly the Recommendation ITU-R P.676-12 and the measured surface meteorological parameters (relative humidity, temperature and pressure). As an example, Fig. 13 depicts the daily behaviour of the meteorological parameters and the gaseous predictions at 39.402 GHz on the 4th of February, 2017.

This article has been accepted for publication in a future issue of this journal, but has not been fully edited. Content may change prior to final publication. Citation information: DOI 10.1109/TAP.2020.3016492, IEEE Transactions on Antennas and Propagation

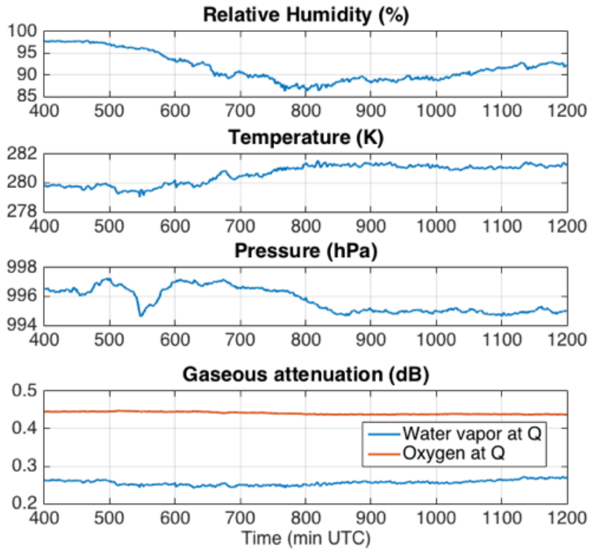

Fig. 13. The meteorological parameters and the gaseous attenuation predictions at 39.402 GHz, Q band (4th of February, 2017).

Thus, the attenuation due to rain and clouds is obtained as:

$$A_{RC}(f_D) = A(f_D) - A_V(f_D) - A_{OX}(f_D) \tag{17}$$

With a limited set of input data, it is necessary to introduce some simplifying hypotheses to separate the attenuation components due to rain and cloud. The proposed method relies on P_0, i.e. the probability to have rain in the observation period associated to the measured attenuation $A(f_D)$ (2017 in this study); P_0 can be calculated from the rain rate time series, if available (note that a simple tipping bucket rain gauge is sufficient to this aim), or extracted, on a yearly basis, from the Recommendation ITU-R P.837-7 [27], which requires as input only the geographical coordinates of the site. Based on P_0, as well as on link elevation angle and on the mean yearly rain height (which can be extracted from the Recommendation ITU-R P.839-4 [28]), the probability to have rain attenuation along the path, P^*_{R0}, can be calculated using the Recommendation ITU-R P.618-13 [3]. For the measurements used in this work, collected in 2017 in Milan, P_0 = 5.2 % (as calculated from the disdrometer-derived rain rate time series), while P^*_{R0} = 7.2 %. As expected $P^*_{R0} > P_0$, because rain might be present along the link but not on the rain gauge.

Starting from the probability that the link is affected by rain attenuation, the algorithm aimed at splitting A_{RC} into A_R and A_C involves the use of a fixed attenuation threshold A_{th}: if $A_{RC} \le A_{th}$, A_{RC} is completely associated to the cloud component A_C; conversely, if $A_{RC} > A_{th}$, part of A_{RC} is ascribed to clouds ($A_C = A_{th}$) and part to rain ($A_R = A_{RC} - A_C$). Fig. 14 summarizes the rain/cloud attenuation separation procedure.

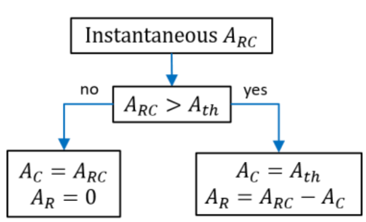

Fig. 14. Procedure to split total attenuation into clouds and rain attenuation, using S-TAFS.

The value of A_{th} is determined by aiming to obtain, from the measured time series of A_{RC}, the probability to have rain attenuation (P_{R0}) that matches the reference one, P^*_{R0}. To this purpose, starting from A_{th} = 0 dB, the value of A_{th} is iteratively increased and the procedure reported in Fig. 14 is applied to the time series of A_{RC} to isolate A_R until $P_{R0} = P^*_{R0}$. With the data considered in this work, A_{th} = 0.26 dB at 19.701 GHz.

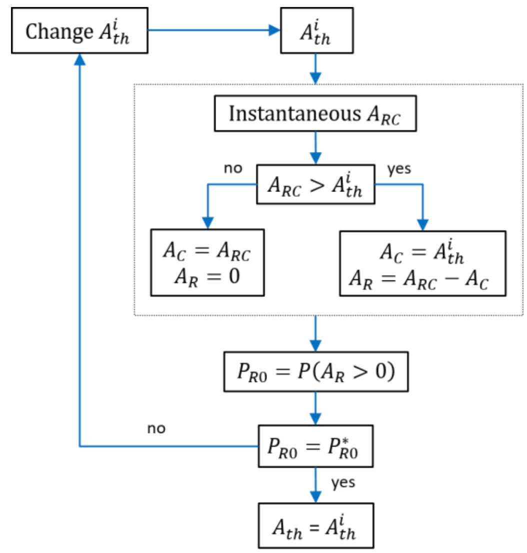

Fig. 15. Workflow to identify the threshold A_{th} to separate cloud attenuation and rain attenuation using S-TAFS.

Fig. 16 summarizes the full procedure to isolate the different attenuation component using S-TAFS, while its application is shown in Fig. 17 for the 4th of February, 2017.

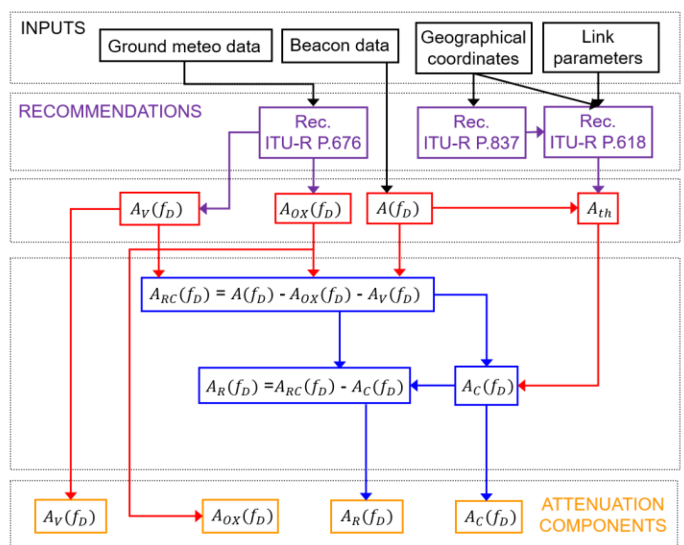

Fig. 16. First part of S-TAFS: derivation of the attenuation due to oxygen, water vapor, clouds and rain from the time series of $A(f_D)$.

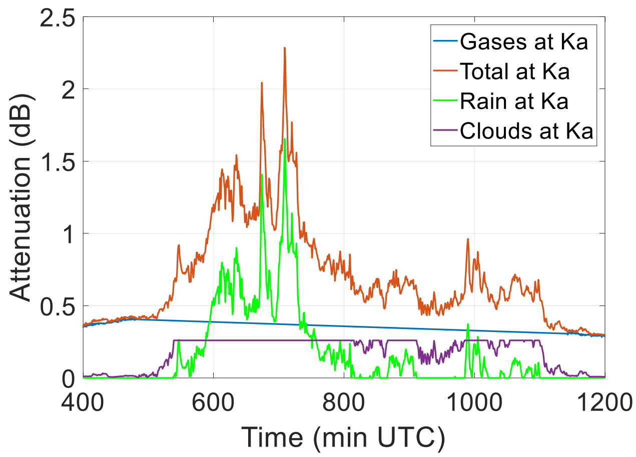

Fig. 17. Separation of the total attenuation (red curve) into its various contributions due to gases (blue curve), clouds (violet curve) and rain (green curve) at 19.701 GHz, using S-TAFS (4th of February, 2017).

B. Frequency Scaling Using S-TAFS

1) Gaseous Attenuation

Given the simplification introduced in S-TAFS, the water vapor and oxygen attenuation at the frequency f_U are simply obtained using again the Recommendation ITU-R P.676-12. As an example, for the 4th of February, 2017, Fig. 18 depicts the water vapor attenuation at both bands, while the time series of the oxygen attenuation are those already shown in Fig. 6.

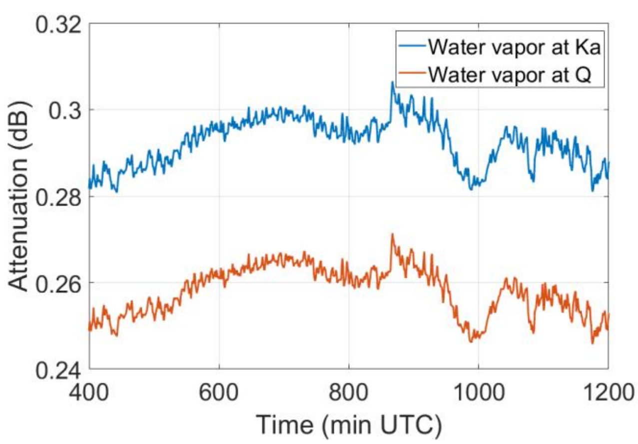

Fig. 18. Scaling the water vapor attenuation from 19.701 GHz (Ka band, blue curve) to 39.402 GHz (Q band, red curve) using S-TAFS (4th of February, 2017).

2) Clouds Attenuation

The procedure to scale clouds attenuation, using (11) and (12), is the same for TAFS and S-TAFS; its application is shown, as an example, in Fig. 19 for the 4th of February, 2017.

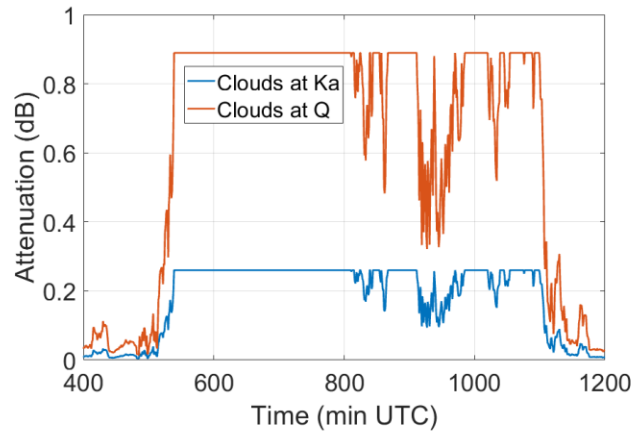

Fig. 19. Scaling the clouds attenuation from 19.701 GHz (Ka band, blue curve) to 39.402 GHz (Q band, red curve) using S-TAFS (4th of February, 2017).

3) Rain Attenuation and Total Attenuation

When rain rate time series are not available, simple rain attenuation scaling models exist, which require as input only the rain attenuation time series $A_R(f_D)$. This is the case of the simple yet effective power law model proposed by Drufuca [5], which is adopted in S-TAFS. In this case $A_R(f_U)$ is calculated as

$$A_R(f_U) = \left(\frac{f_U}{f_D}\right)^{1.72} A_R(f_D) \tag{18}$$

On the other hand, if rain rate time series are available, a higher accuracy can be achieved by exploiting the Enhanced Synthetic Storm Technique (E-SST) [16], which improves the Synthetic Storm Technique (SST) [29], by embedding a simple algorithm to distinguish between stratiform and convective events for a selective inclusion of the additional attenuation induced by the melting layer. Moreover, the velocity of translation of each event over the site depends on the hourly values of the wind intensity w extracted from the ERA5 database (associated to the 700-mbar isobar), which is also the source used to derive the hourly values of the rain height h_R used as input to E-SST. The results in [16] indicate that, using the rain rate time series as input to E-SST to calculate the rain attenuation at the two bands, it is possible to define the following frequency scaling ratio:

$$R_{FS}^{E-SST} = \frac{A_R^{E-SST}(f_U)}{A_R^{E-SST}(f_D)} \tag{19}$$

which provides almost the same scaling accuracy as the ratio defined in (14). Differently from what is done in [16], in this work, in order to limit the complexity of S-TAFS, as well as the need of elaborated input data, the E-SST predictions in S-TAFS ($A_R^{E-SST}(f_D)$and $A_R^{E-SST}(f_U)$) are achieved using as input to the model only the mean yearly ERA5 values of h_R and w, rather than the hourly values.

This article has been accepted for publication in a future issue of this journal, but has not been fully edited. Content may change prior to final publication. Citation information: DOI 10.1109/TAP.2020.3016492, IEEE Transactions on Antennas and Propagation

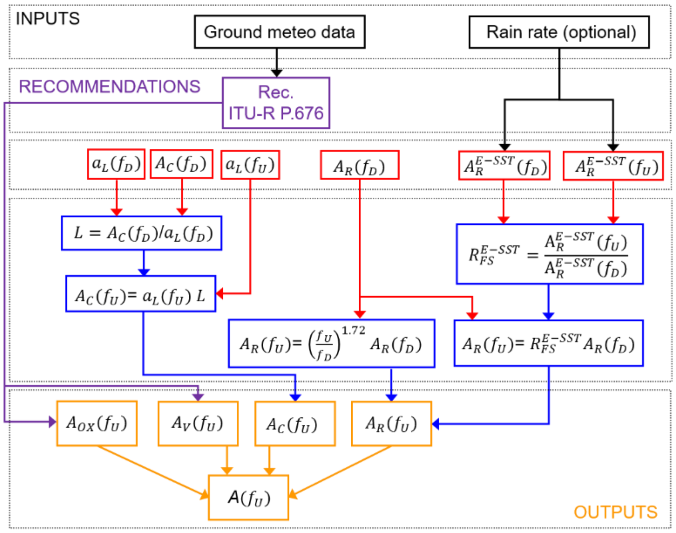

Fig. 20. Second part of S-TAFS: how oxygen, water vapor, clouds and rain attenuation time series are scaled to the target frequency f_{UP}.

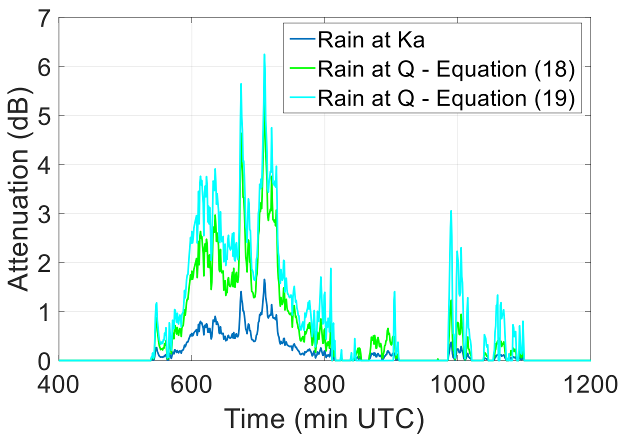

Fig. 21. Scaling the rain attenuation from 19.701 GHz (Ka band, blue curve) to 39.402 GHz (Q band, red and green curves) using S-TAFS (4th of February, 2017), considering both scaling methods for the rain component.

Similarly to TAFS, $A(f_U)$ is calculated by summing up all the attenuation components using (13). Fig. 20 resumes the frequency scaling procedure of S-TAFS, while Fig. 21 depicts the time series of rain attenuation scaled from Ka band to Q band using S-TAFS for the 4th of February, 2017, achieved by employing both scaling rationships in (18) and (19). Finally, Fig. 22 depicts the time series of $A(f_U)$ for the same day using (18) to scale rain attenuation.

Given its simplicity and the limited complexity of its input data, S-TAFS is applicable not only to obtain attenuation statistics and time series for the design of satellite communication systems at higher frequencies, but to operate, almost in real time, a fade mitigation technique (e.g. Up Link Power Control) in real systems.

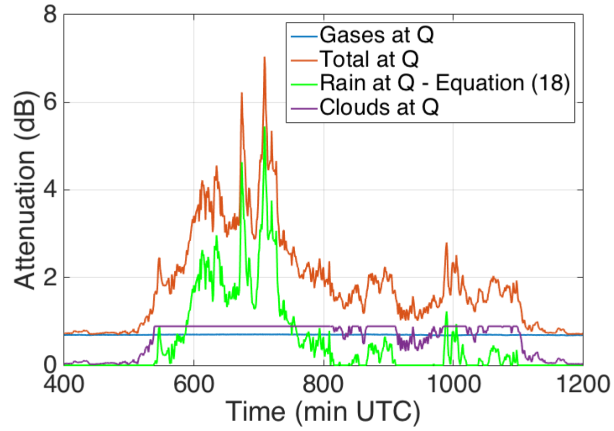

Fig. 22. Gases (blue curve), clouds (violet curve), rain (green curve) and total attenuation (red curve) at 39.402 GHz scaled from the corresponding values at 19.701 GHz using S-TAFS (4th of February, 2017); equation (18) is used to scale rain attenuation.

V. Results and Discussion

This section focuses on assessing the accuracy of TAFS and S-TAFS in predicting total tropospheric attenuation. The tests are performed by exploiting the full year (2017) of propagation data collected in Milan using the NASA equipment presented in Section II. Total attenuation data at 19.701 GHz are used as input to TAFS and S-TAFS to predict total attenuation at 39.401 GHz, which is compared to the measured total attenuation at the same frequency.

Fig. 23 compares the CCDF of scaled and measured total attenuation at 39.402 GHz in 2017.

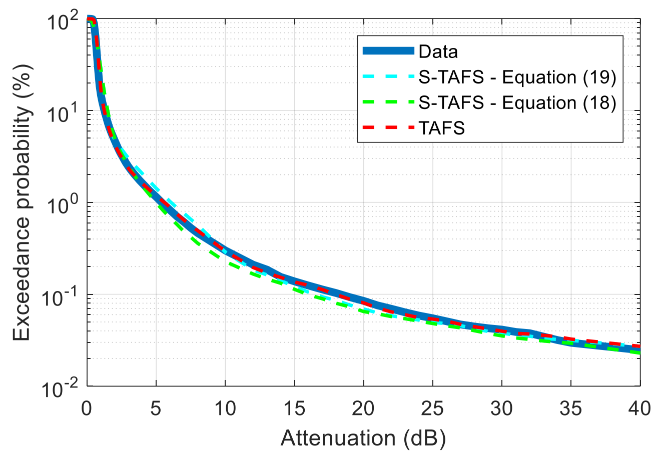

Fig. 23. Application of TAFS and S-TAFS to scale total attenuation from 19.701 GHz to 39.402 GHz; the CCDFs are calculated for the whole year 2017.

As expected, the best accuracy is achieved through TAFS while, due its simplified approach, S-TAFS offers a slightly lower prediction performance. This conclusion is confirmed by the results reported in Table IV, which lists the mean (E) and root mean square (RMS) value of the error figure inspired by the one defined by ITU-R in [30] for attenuation measurements:

$$\varepsilon(P) = \begin{cases} 100 \cdot \left(\frac{A(P)}{10}\right)^{0.2} \ln\left(\frac{A_P(P)}{A_R(P)}\right) & A_R(P) < 10 \text{ dB} \\ 100 \cdot \ln\left(\frac{A_P(P)}{A_R(P)}\right) & A_R(P) \geq 10 \text{ dB} \end{cases} \quad (20)$$

This article has been accepted for publication in a future issue of this journal, but has not been fully edited. Content may change prior to final publication. Citation information: DOI 10.1109/TAP.2020.3016492, IEEE Transactions on Antennas and Propagation

In (20), $A_R(P)$ and $A_P(P)$ represent, respectively, the measured and scaled total attenuation exceeded for the time percentage P.

Moreover, the frequency scaling approach for rain attenuation based on (18) obviously provides a lower prediction accuracy (due to the use of a constant rain attenuation scaling ratio), but its performance is very close to the one of E-SST based approach; this very positive outcome indicates that even without the need of rain rate time series, very satisfactory results can be achieved.

TABLE IV. OVERALL PREDICTION ACCURACY OF TAFS AND S-TAFS (BOTH APPROCHES FOR RAIN ATTENUATION FREQUENCY SCALING ARE REPORTED): TOTAL ATTENUATION CCDFS (2017) AT 39.402 GHZ (Q BAND).

	E (%)	RMS (%)
TAFS	-0.16	1.72
S-TAFS – Equation (19)	-0.32	4.22
S-TAFS – Equation (18)	-1.05	4.7

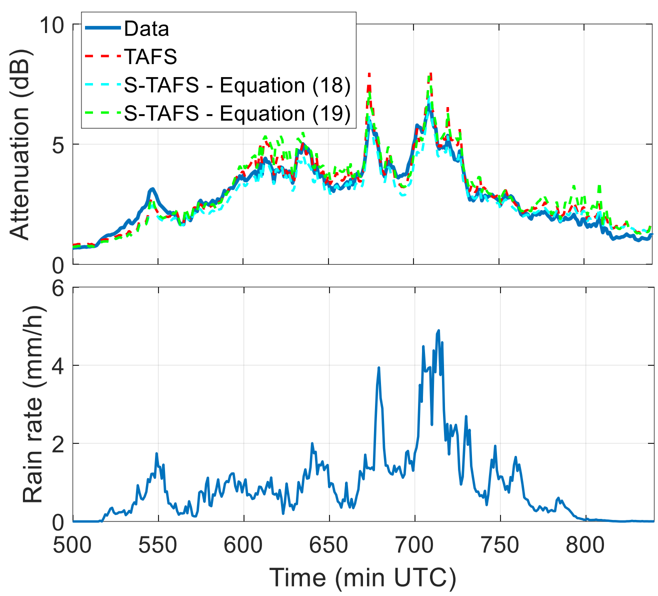

Fig. 24. Application of TAFS and S-TAFS to scale the total tropospheric attenuation from Ka band to Q band, for the 4th of February 2017 (stratiform event).

The increased accuracy of TAFS is corroborated also by the tests performed on the time series of total attenuation, which are crucial for the design of the necessary fade mitigation techniques, in turn required when fixed power margins are no longer sufficient to provide the expected system performance. As an example, Fig. 24 compares the estimated and measured time series of total attenuation (4th of February, 2017) at 39.402 GHz for a stratiform rain event. On the other hand, Fig. 25 offers an example of the models' performance for a convective event occurred on the 2nd of May, 2017. Also in this case, both TAFS and S-TAFS provide accurate predictions.

The very satisfactory performance of TAFS and S-TAFS is confirmed by Table V, which lists E and RMS of the absolute error figure defined as:

$$\phi(t) = A_P(t) - A_R(t) \quad (21)$$

which is calculated considering all the data collected in 2017. The overall RMS value is lower than 0.5 dB.

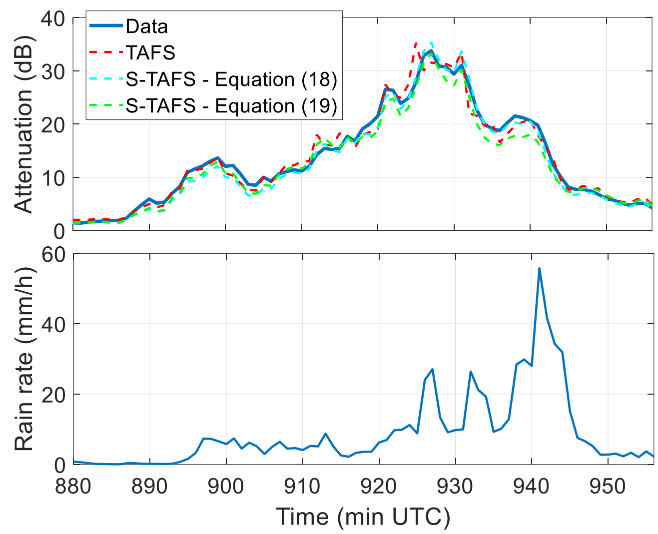

Fig. 25. Application of TAFS and S-TAFS to scale the total tropospheric attenuation from Ka band to Q band, for the 4th of February 2017 (convective event).

TABLE V. OVERALL PREDICTION ACCURACY OF TAFS AND S-TAFS (BOTH APPROCHES FOR RAIN ATTENUATION FREQUENCY SCALING ARE REPORTED): TOTAL ATTENUATION TIME SERIES (2017), Q BAND.

	E (dB)	RMS (dB)
TAFS	0.05	0.38
S-TAFS – Equation (19)	0.01	0.43
S-TAFS – Equation (18)	0.06	0.41

VI. CONCLUSIONS

This paper presents the development of two methodologies (TAFS and S-TAFS) aimed at up-scaling in frequency (e.g. up to W band) the total tropospheric attenuation time series measured at a lower frequency (e.g. Ka band). Both methods include a procedure to isolate the attenuation induced by the different atmospheric constituents, each of which is separately up-scaled to the target frequency with a solid physically-based approach. Though more accurate, TAFS requires more detailed information as inputs (e.g. radiometric and disdrometer data); on the other hand S-TAFS makes use of limited inputs and it is based on simplified assumptions, which reflect in a slightly worse performance, but also in a wider applicability. In order for S-TAFS to be applicable to as many sites as possible, it does not strictly require the rain rate time series as input, though better results are achievable with such input data.

Tests against the propagation data collected in Milan in the framework of the Alphasat Aldo Paraboni experiment indicate that, on first-order statistics, TAFS provides an RMS error of 1.72%, while that associated to S-TAFS ranges between 4.22% and 4.7%. Similar results are obtained for instantaneous predictions, which are key for the design and operation of Fade Mitigation Techniques (FMTs): the average RMS of the error on the time series was found to be 0.38 dB for TAFS, while it varies between 0.41 dB and 0.43 for E-SST.

The results achieved in this work suggest that TAFS and S-TAFS can be used to predict the total tropospheric attenuation at much higher frequencies (e.g. the W band), for which no measurements are currently available, starting from the largely available Ka band measurements. However, to this aim, further tests are required to assess the accuracy of TAFS and S-TAFS: indeed, scaling rain attenuation to much higher frequencies, especially using the simplified approaches proposed for S-TAFS, is expected to become more and more critical as the frequency increases. Moreover, the applicability of TAFS to other sites requires the recalculation of the cloud attenuation ratio R_{RC} in (7), which is expected to depend on the local climate, but also on the link frequency and elevation angle. This is one of the reasons why a simpler version of TAFS was devised, S-TAFS, which is expected to be more widely applicable.

Acknowledgment

The authors would like to acknowledge: the Agenzia Spaziale Italiana (ASI), in particular Giuseppe Codispoti, for supporting the Alphasat Aldo Paraboni propagation experiment; NASA for making available the experimental data within the collaboration with Politecnico di Milano on the Alphasat Aldo Paraboni propagation experiment; ECMWF for providing vertical atmospheric profiles.

This effort was supported in part by the Air Force Office of Scientific Research, Air Force Material Command, USAF, under grant number FA9550-17-1-0335. The U.S Government is authorized to reproduce and distribute reprints for Governmental purpose notwithstanding any copyright notation thereon.

References

[1] T. Rossi, F. Maggio, M. De Sanctis, M. Ruggieri, S. Falzini, M. Tosti, “System analysis of smart gateways techniques applied to Q/V-band high throughput satellites,” *IEEE Aerospace Conference*, pp. 1-10, 1-8 March 2014, Big Sky, Montana, USA.

[2] C. Riva, C. Capsoni, L. Luini, M. Luccini, R. Nebuloni, A. Martellucci, “The Challenge of Using the W Band in Satellite Communication,” *International Journal of Satellite Communications and Networkorking*, 32(3), 2014, pp. 187–200.

[3] Recommendation ITU-R P.618-13, “Propagation data and prediction methods required for the design of Earth-space telecommunication systems,” December 2017.

[4] Recommendation ITU-R P.1853-2, “Time series synthesis of tropospheric impairments,” August 2019.

[5] G. Drufuca, “Rain attenuation statistics for frequencies above 10 GHz from rain gauge observations,” Journal of Geophysical Research: Atmospheres, 1-2, 1974, pp. 399-411.

[6] D. Hodge, "Frequency scaling of rain attenuation," in IEEE Transactions on Antennas and Propagation, vol. 25, no. 3, pp. 446-447, May 1977, doi: 10.1109/TAP.1977.1141580.

[7] B. C. Grémont, "On the frequency scaling of rain attenuation for space communications," 2009 Loughborough Antennas & Propagation Conference, Loughborough, 2009, pp. 185-188.

[8] S. Bertorelli, A. Paraboni, ‘Modelling of short-term frequency scaling for rain attenuationusing ITALSAT data’, International Journal of Satellite Communications and Networking, 25, 2006, pp. 251-262.

[9] O. Brisseau, C. Mallet, L. Barthes, T. Marsault, ‘Frequency scaling of rain attenuation based on microphysical characteristics for SatCom links’, IEE Proceedings - Microwaves, Antennas and Propagagation, 153(6), 2006, pp. 523-532.

[10] J. Nessel, M. Zemba, L. Luini, C. Riva, “Comparison of Instantaneous Frequency Scaling from Rain Attenuation and Optical Disdrometer Measurements at K/Q bands,” 21st Ka and Broadband Communications, Navigation and Earth Observation Conference, Bologna (Italy), pp. 1-10, 12-14 October, 2015.

[11] F. Cuervo, K. Plimon, M. Schönhuber, A. Martellucci and J. R. Castro, "Alphasat Aldo Paraboni propagation experiment in Graz - frequency scaling analysis," 2016 10th European Conference on Antennas and Propagation (EuCAP), Davos, 2016, pp. 1-5.

[12] T. Rossi, M. De Sanctis, M. Ruggieri, C. Riva, L. Luini, G. Codispoti, E. Russo, G. Parca, “Satellite Communication and Propagation Experiments Through the Alphasat Q/V Band Aldo Paraboni Technology Demonstration Payload,” *IEEE Aerospace and Electronic Systems Magazine*, 31(3), March 2016 pp. 18–27.

[13] L. Luini, G. Roveda, M. Zaffaroni, M. Costa, C. Riva, “The Impact of Rain on Short E-band Radio Links for 5G Mobile Systems: Experimental Results and Prediction Models,” accepted for publication in IEEE Transactions on Antennas and Propagation.

[14] L. Luini, C. Riva, R. Nebuloni, M. Mauri, J. Nessel, A. Fanti, “Calibration and Use of Microwave Radiometers in Multiple-site EM Wave Propagation Experiments,” *EuCAP 2018*, 9-13 April 2018, pp. 1-5, London, UK.

[15] X. Boulanger, B. Gabard, L. Casadebaig, L. Castanet, “Four Years of Total Attenuation Statistics of Earth-Space Propagation Experiments at Ka-Band in Toulouse,” *IEEE Transactions on Antennas and Propagation*, 63(5), May 2015, pp. 2203-2214.

[16] L. Luini, C. Riva, A. Panzeri, “Enhancement of the Synthetic Storm Technique for the Prediction of Rain Attenuation Time Series at EHF,” accepted for publication in IEEE Transactions on Antennas and Propagation

[17] Recommendation ITU-R P.840-7, “Attenuation due to clouds and fog,” December 2017.

[18] L. Luini, C. Riva, C. Capsoni, A. Martellucci, “Attenuation in non rainy conditions at millimeter wavelengths: assessment of a procedure,” IEEE Transactions on Geoscience and Remote Sensing, 45(7), July 2007, pp. 2150-2157.

[19] E. Salonen, W. Uppala, “New prediction method of cloud attenuation,” *Electronics Letters*, 27(12), 1991, pp. 1106–1108.

[20] H. J. Liebe, G. A. Hufford, M. G. Cotton, ”Propagation modelling of moist air and suspended water/ice particles at frequencies below 1000 GHz,” *AGARD 52nd Specialists’ Meeting of The EM Wave Propagation Panel*, Palma De Maiorca, Spain, 1993.

[21] Recommendation ITU-R P.676-12, “Attenuation by atmospheric gases,” Geneva, 2019.

[22] L. Luini, C. Riva, “Improving the Accuracy in Predicting Water Vapor Attenuation at Millimeter-wave for Earth-space Applications,” *IEEE Transactions on Antennas and Propagation*, vol. 64, no. 6, Page(s): 2487 - 2493, June 2016.

[23] L. Luini, C. Capsoni, “Efficient Calculation of Cloud Attenuation for Earth-space Applications,” *IEEE Antennas and Wireless Propagation Letters*, vol. 13, Page(s): 1136 - 1139, 2014.

[24] M. Mishchenko, L. Travis, A. Lacis, “Scattering, Absorption, and Emission of Light by Small Particles,” *Cambridge University*, 2002.

[25] K. Beard, C. Chuang, “A New Model for the Equilibrium Shape of Raindrops,” *Journal of the Atmospheric Sciences*, 44(11), 1987, pp. 1509–1524.

[26] L. Luini, G. A. Siles, J. M. Riera, C. Riva, J. Nessel, “Methods to Estimate Gas Attenuation in Absence of a Radiometer to Support Satellite Propagation Experiments,” *accepted for publication in IEEE Transactions on Instrumentation and Measurements*.

[27] Recommendation ITU-R P.837-7, “Characteristics of precipitation for propagation modelling,” Geneva, 2017.

[28] Recommendation ITU-R P.839-4, “Rain height model for prediction methods,” Sepember 2013.

[29] E. Matricciani, “Physical-mathematical model of the dynamics of rain attenuation based on rain rate time series and two layer vertical structure of precipitation,” *Radio Science*, 31(2), March-April 1996, pp. 281-295.

[30] Recommendation ITU-R P.311-14, “Acquisition, presentation and analysis of data in studies of radiowave propagation,” Geneva, 2013.